

(2)

GL-TR-90-0026

DTIC FILE COPY

DEMONSTRATE THE FEASIBILITY OF A DETECTION METHOD TO SEPARATE  
NEUTRAL PARTICLES FROM CHARGED PARTICLES IN THE MEV/NUCLEON  
ENERGY RANGE

Bronislaw K. Dichter  
Frederick A. Hanser

PANAMETRICS, INC.  
221 Crescent Street  
Waltham, MA 02254

February 1990

Final Scientific Report  
July 1988 - December 1989

Approved for Public Release; Distribution Unlimited

GEOPHYSICS LABORATORY  
AIR FORCE SYSTEMS COMMAND  
UNITED STATES AIR FORCE  
HANSCOM AFB, MA 01731-5000

00 08 22 050

DTIC  
ELECTE  
AUG 23 1990  
S D D  
Co


AD-A225 656

This technical report has been reviewed and is approved for publication.

  
MARILYN R. OBERHARDT  
Contract Manager

  
E.G. MULLEN  
Branch Chief

FOR THE COMMANDER

  
RITA C. SAGALYN  
Space Physics Division Director

This report has been reviewed by the ESD Public Affairs Office (PA) and is releasable to the National Technical Information Service (NTIS).

Qualified requestors may obtain additional copies from the Defense Technical Information Center. All others should apply to the National Technical Information Service.

If your address has changed, or if you wish to be removed from the mailing list, or if the addressee is no longer employed by your organization, please notify GL/IMA, Hanscom AFB, MA 01731. This will assist us in maintaining a current mailing list.

Do not return copies of this report unless contractual obligations or notices on a specific document requires that it be returned.

UNCLASSIFIED

SECURITY CLASSIFICATION OF THIS PAGE

## REPORT DOCUMENTATION PAGE

1a. REPORT SECURITY CLASSIFICATION Unclassified			1b. RESTRICTIVE MARKINGS	
2a. SECURITY CLASSIFICATION AUTHORITY			3. DISTRIBUTION/AVAILABILITY OF REPORT Approved for public release; Distribution unlimited	
2b. DECLASSIFICATION/DOWNGRADING SCHEDULE				
4. PERFORMING ORGANIZATION REPORT NUMBER(S)			5. MONITORING ORGANIZATION REPORT NUMBER(S) GL-TR-90-0026	
6a. NAME OF PERFORMING ORGANIZATION Panametrics, Inc.		6b. OFFICE SYMBOL (If applicable)	7a. NAME OF MONITORING ORGANIZATION Geophysics Laboratory	
6c. ADDRESS (City, State and ZIP Code) 221 Crescent Street Waltham, MA 02254			7b. ADDRESS (City, State and ZIP Code) Hanscom AFB Massachusetts 01731-5000	
8a. NAME OF FUNDING/SPONSORING ORGANIZATION		8b. OFFICE SYMBOL (If applicable)	9. PROCUREMENT INSTRUMENT IDENTIFICATION NUMBER F19628-87-C-0126	
8c. ADDRESS (City, State and ZIP Code)			10. SOURCE OF FUNDING NOS.	
			PROGRAM ELEMENT NO. 62101F	PROJECT NO. 7601
			TASK NO. 12	WORK UNIT NO. CA
11. TITLE (Include Security Classification) Demonstrate the Feasibility of a (cont'd back)				
12. PERSONAL AUTHOR(S) Bronislaw K. Dichter, Frederick A. Hanser				
13a. TYPE OF REPORT Scientific Report #2		13b. TIME COVERED FROM JUL 88 TO DEC 89		14. DATE OF REPORT (Yr., Mo., Day) 1990 February
15. PAGE COUNT 42				
16. SUPPLEMENTARY NOTATION				
17. COSATI CODES			18. SUBJECT TERMS (Continue on reverse if necessary and identify by block number)	
FIELD	GROUP	SUB. GR.	Convoy Electrons, Charged/Neutral Particles Differentiation Neutral Particle Beams, Space Instrumentation, Feasibility Study, Broadband Noise, CP	
19. ABSTRACT (Continue on reverse if necessary and identify by block number) A breadboard model of a spacecraft borne instrument to measure neutral hydrogen atomic fluxes with energies between 1 to 10 MeV/nucleon has been designed, constructed and tested. Differentiation between incident charged and neutral particles was accomplished by measuring the production rate of convoy electrons by the particles. Convoy electron production rate is much larger for neutral hydrogen than for protons. Incident particles strike a thin carbon foil at the entrance aperture and the resulting convoy electrons are deflected by an applied electrostatic field and detected by a micro channel plate detector. The forward going protons are undeflected by the electric field and are detected in a solid state detector. The instrument has been tested with accelerator proton and atomic hydrogen beams of 1.5 to 4 MeV energy. Experimental results and theoretical model calculations are compared. A design for an improved spacecraft instrument is presented. <i>Kell...</i>				
20. DISTRIBUTION/AVAILABILITY OF ABSTRACT UNCLASSIFIED/UNLIMITED <input checked="" type="checkbox"/> SAME AS RPT <input type="checkbox"/> DTIC USERS <input type="checkbox"/>			21. ABSTRACT SECURITY CLASSIFICATION UNCLASSIFIED	
22a. NAME OF RESPONSIBLE INDIVIDUAL Marilyn Oberhardt, 1Lt., USAF			22b. TELEPHONE NUMBER (Include Area Code) (617) 377-3857	22c. OFFICE SYMBOL AFGL/PHP

UNCLASSIFIED

SECURITY CLASSIFICATION OF THIS PAGE

11. Title (Cont'd)

Detection Method to Separate Neutral Particles from Charged Particles in the MeV/  
Nucleon Energy Range

UNCLASSIFIED

SECURITY CLASSIFICATION OF THIS PAGE

## Table of Contents

TABLE OF FIGURES	iv
TABLE OF TABLES	vi
1. INTRODUCTION	1
2. THEORETICAL CALCULATIONS	2
2.1 Neutral Beams	2
2.1.1 Neutral Fraction Following Beam-Foil Interaction	3
2.1.2 Neutral Beam Transport	5
2.2 Convoy Electron Production Model	6
3. EXPERIMENTAL EQUIPMENT	8
3.1 Magnetic Analyzer Breadboard Instrument	8
3.2 Electrostatic Breadboard Instrument	11
3.3 Accelerator Test Setup	14
4. EXPERIMENTAL RESULTS AND DATA ANALYSIS	17
4.1 Magnetic Device - Experimental Results	17
4.2 Electrostatic Device - Experimental Results	18
4.2.1 MCP Position Spectra	19
4.2.2 Experimental and Calculated Electron Yields	21
4.2.3 Electron Yields Without Stripper Foil	24
4.3 Summary of Results	27
5. PRELIMINARY ENGINEERING MODEL DESIGN	27
5.1 Mechanical Design	28
5.2 Performance Characteristics	31
6. CONCLUSIONS	35
REFERENCES	36

## Table of Figures

Figure 2.1	Electron loss and capture cross sections calculated using eqs. (2.2) and 2.3).	4
Figure 2.2	Calculated convoy electron production rates per incident beam particle.	8
Figure 3.1	Schematic diagram of the magnetic analyzer instrument.	9
Figure 3.2	Schematic diagram of the electrostatic breadboard instrument.	11
Figure 3.3	Calculated equipotential surfaces of the electrostatic instrument.	12
Figure 3.4	Allowed energy-angle combinations for electrons that strike the MCP.	14
Figure 3.5	Experimental setup at University of Lowell beam tests.	14
Figure 3.6	Beam energy profiles as measured by the solid state detector for a 1.5 MeV beam.	15
Figure 4.1	Singles MCP spectrum: neutral beam, 4 MeV beam energy.	20
Figure 4.2	Coincidence MCP spectrum: neutral beam, 4 MeV beam energy.	20
Figure 4.3	Coincidence MCP spectrum: charged beam, 4 MeV beam energy.	21
Figure 4.4	Measured and calculated values of $\delta R$ . Calculation parameters: $\epsilon = 0.045$ , $L_{\text{eff}} = 58 \text{ \AA}$ .	24

Figure 4.5	Measured and calculated values of $\delta R$ . Calculation parameters: $\epsilon = 0.015$ , $L_{eff} = 121 \text{ \AA}$ .	25
Figure 4.6	Measured and calculated values of $\delta R$ . Calculation parameters: $\epsilon = 0.070$ , $L_{eff} = 40 \text{ \AA}$ .	25
Figure 4.7	Coincidence MCP position spectrum: Neutral beam, 4 MeV beam energy, no carbon foil.	26
Figure 4.8	Coincidence MCP position spectrum: charged beam, 4 MeV beam energy, no carbon foil.	26
Figure 5.1	Engineering model - version A.	29
Figure 5.2	Engineering model - version B.	30

Accession For	
NTIS CRA&I	<input checked="" type="checkbox"/>
DTIC TAB	<input type="checkbox"/>
Unannounced	<input type="checkbox"/>
Justification	
By	
Distribution /	
Availability Codes	
Dist	Avail and/or special
A-1	

## Table of Tables

Table 3.1	Calculated and measured energy separation between particles that traverse the foil and those that travel through the pinholes in the foil.	17
Table 4.1	Listing of beam energies and foils used during experiments.	19
Table 4.2	Electron yields measured with the electrostatic instrument.	22
Table 4.3	Summary of results obtained with no stripping foil.	26
Table 5.1	Minimum number of incident particle counts required to determine a given neutral-charged particle flux ratio.	34



## 1. INTRODUCTION

The detection and identification of neutral atoms such as hydrogen or helium, with energies of 1 MeV/nucleon and higher, by spacecraft borne instruments is likely to become important in the future. Solid state detector telescopes can readily detect incident neutrals but, since all incident atomic ions and neutrals rapidly achieve charge state equilibrium upon entering matter, it is not possible to distinguish between incoming neutral and charged particles solely with solid state telescopes. Neutral and charged particles can be separated by electric and magnetic fields. In the MeV/nucleon range, however, this method requires strong fields over large distances and so is not suitable for spacecraft instruments where weight and size are generally limited. This report describes the progress made in designing and testing a comparatively small and light weight detection system that can statistically separate neutral and charged particles. The possible uses of such a system are to monitor space based tests of neutral beam systems, to monitor the exposure of satellites to neutral particle beams and to monitor the naturally occurring neutral particle flux in space.

The instruments used in the work described in this report use a solid state detector to measure the energy of an incident beam particle. In addition, a micro channel plate (MCP) is used to detect energetic, forward moving electrons, convoy electrons, produced by the passage of the incident particle through a thin carbon foil located in front of the detector. The convoy electron yield is expected to be much larger for incident neutral particles than it is for incident charged particles. This difference in yield can provide the desired signature of incident neutral particles.

This report contains the results of theoretical calculations and experimental work with a breadboard model of a neutral atom detector. Section 2 is devoted to the description of a simple model of convoy electron production. In addition, a method of obtaining and transporting a neutral atomic hydrogen beam with an energy of several MeV is described. The instruments used in the experimental phase of this work, as well as the setup used for beam tests of the instruments at the University of Lowell Van de Graaff accelerator, are described in Section 3. Section 4 contains a detailed overview of the collected data and comparisons of the data with the results of the calculations from Section 2. Preliminary

designs for two versions of the engineering model of the flight instrument are presented in Section 5. Summary and conclusions of this report are included in Section 6.

## 2. THEORETICAL CALCULATIONS

### 2.1 Neutral Beams

In order to produce neutral beam bombardment of the detector, the neutral particles must be produced in the neutralizing foil and the resulting beam must be transported to the detector. The following two sections will be concerned with the production and transport of the neutral beams. Some of the derived results will be used in the subsequent discussion of convoy electron production.

#### 2.1.1 Neutral Fraction Following Beam-Foil Interaction

Neutral particles are produced by the pickup of the foil electrons by charged beam particles. A singly charged particle moving through a medium has a cross section for electron capture,  $\sigma_c$ , and, once it has captured an electron, a cross section for its subsequent loss,  $\sigma_l$ . It can be directly shown that the neutral fraction,  $f_0$ , of an initially charged beam after traversing a distance  $x$  in a foil is given by

$$f_0(x) = \frac{\sigma_c}{\sigma_l + \sigma_c} \cdot [1 - \exp\{-(\sigma_l + \sigma_c)Nx\}] \quad , \quad (2.1)$$

where  $N$  is density of atoms of the foil material.

The capture and loss cross sections for protons can be expressed as functions of proton velocity using the Brandt-Sizmann theory (Ref. 2.1):

$$\sigma_c = 5.24 \cdot 10^4 \pi a_0^2 Z^5 V^{-6} \cdot [V^2 + 18.71 \cdot Z^{14/9}]^{-3} \quad (2.2)$$

$$\sigma_l = \pi a_0^2 \cdot \frac{Z^{2/3}}{Z^{2/3} + V} \cdot \frac{4Z^{1/3}(Z + 1)}{4Z^{1/3}(Z + 1) + V} \quad (2.3)$$

where  $a_0$  is the Bohr radius,  $Z$  is the atomic number of the foil material and  $V$  is the velocity in atomic units (atomic velocity unit =  $2.18 \cdot 10^8$  cm/sec). Evaluating equations (2.2) and (2.3) shows that  $\sigma_l$  is of the order of  $10^{-17}$  cm<sup>2</sup> for proton energies between 1 and 20 MeV while  $\sigma_c$  decreases rapidly from  $10^{-20}$  to  $10^{-25}$  cm<sup>2</sup> in the same energy range (see Figure 2.1). Therefore, for foils thick enough to permit charge equilibration, equation (2.1) reduces to

$$f_0 = \sigma_c / \sigma_l \quad (2.4)$$

since  $\sigma_l \gg \sigma_c$ . The neutralizing foil to be used in this work is a 0.15 mil Al, so that the equilibration condition is satisfied.

### 2.1.2 Neutral Beam Transport

In addition to producing a neutral beam component, the beam-foil interaction also produces angular dispersion of the beam by the process of multiple scattering. The root-mean-square (rms) scattering angle,  $\theta_{rms}$  of a protons incident on a target with atomic number  $Z$  and areal density of atoms  $N$  is given by (Ref.2.2)

$$\theta_{rms} = \frac{\pi N Z (Z + 1) e^4}{E^2} \cdot \ln \left( \frac{4 \pi N a_0}{1 + Z^{2/3}} \cdot \frac{Z + 1}{Z} \right) \quad (2.5)$$

where  $e$  is the electron charge. The angular distribution is to a good approximation a Gaussian, with the standard deviation well approximated by  $\theta_{rms}$ . The angular spread of the neutral beam

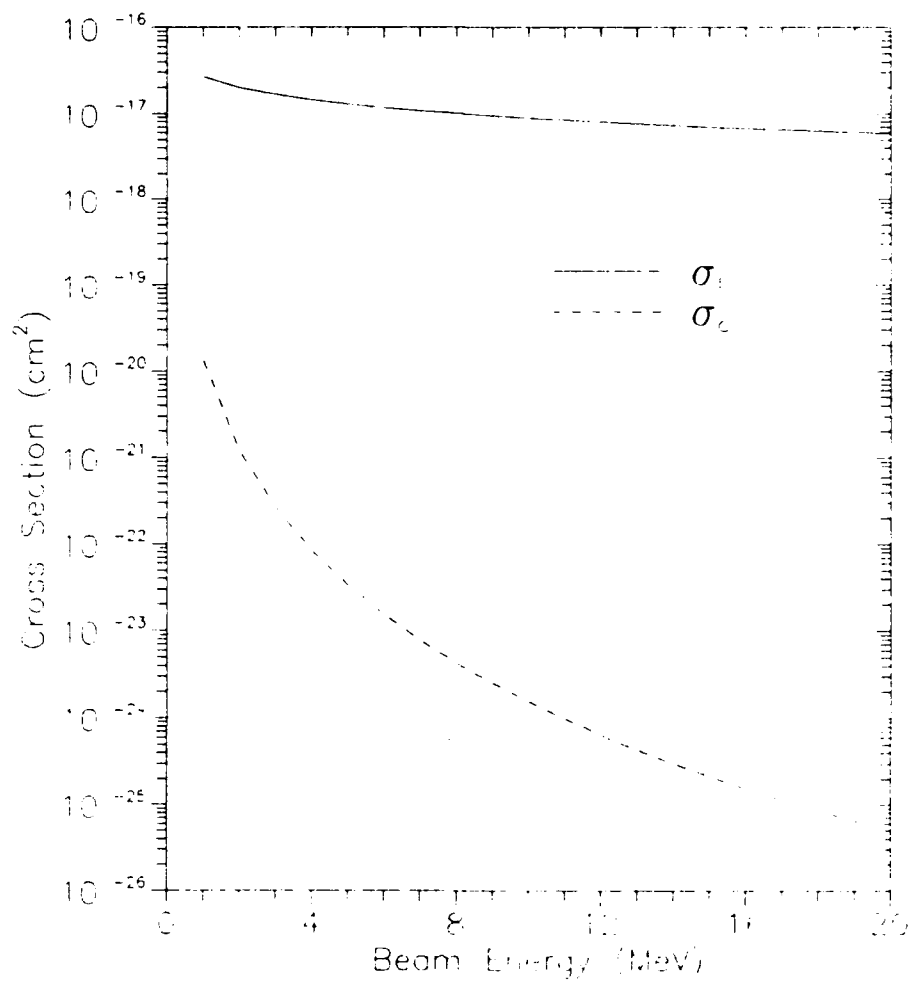


Figure 2.1 Electron loss and capture cross sections calculated using eqs. (2.2) and (2.3).

component may be somewhat different from that of the charged component since there exist two additional effects that contribute to scattering of the neutral particles. One effect, the decrease in multiple Coulomb scattering for neutral particles, will tend to make the rms scattering angle smaller while the other, pickup of transverse angular momentum during electron capture, will tend to make it larger. Both effects are small in magnitude at the beam energies of interest and eq. (2.5) can be expected to be a good estimate of the rms scattering angle for the neutral beam.

The distance between the beam neutralization foil and the detector is large. At the University of Lowell accelerator facility this distance is approximately 10 feet. This is due to the fact that the beam must go through a large dipole electromagnet which bends the charged beam component away from the detector. The entrance aperture to the detector has a diameter of 3 mm, so that even the small rms scattering angle, typically of the order of  $0.03^\circ$ , can lead to a large loss of neutral beam intensity in the detector. Therefore, a correction to the neutral yield calculated with eq. (2.4) must be made to include effects of beam dispersion.

## 2.2 Convoy Electron Production Model

The expected yields of convoy electrons for incident protons and neutral atomic hydrogen can be calculated using a simple model of convoy electron production. The model assumptions are as follows.

- 1) Convoy electron candidates are produced by stripping electrons from neutral hydrogen atoms traversing the target.
- 2) Once an electron is stripped off, it moves initially with the projectile velocity but suffers angular scattering and energy straggling due to collisions with the target atoms.

In view of the first assumption incident protons can only produce convoy electrons following a capture of a foil electron.

Consequently, convoy electron yield per incident beam particle with a velocity  $V$ ,  $N_e(V)$ , can be expressed, within the framework of this model, by

$$N_e(V) = \int_0^{x_0} F(x,V) \cdot P_e(x_0-x,V) dC(x,V) \quad (2.6)$$

where  $x_0$  is the foil thickness,  $F(x,V)$  is the fraction of particles in the neutral state at a distance  $x$  in the foil,  $P_e(x_0-x,V)$  is the electron transmission probability and  $dC(x)$  is the probability of a beam particle undergoing an electron-stripping collision in a section of foil, between  $x$  and  $x + dx$ .

The expressions for the neutral fraction of the beam are taken from the work of Gaillard *et al.* (Ref. 2.3). For an incident neutral atomic hydrogen beam, the neutral fraction,  $F_H$ , as function of time of transit through the foil,  $t_d$ , is given by

$$F_H(t_d) = f_0 + (1 - f_0) \exp(-t_d/t_0) \quad (2.7)$$

while for an incident proton beam the expression is

$$F_p(t_d) = f_0(1 - \exp(-t_d/t_0)) \quad (2.8)$$

where  $f_0$  is given by eq. (2.4) and  $t_0$  is the effective neutral hydrogen "lifetime" in the foil. Gaillard *et al.* (Ref. 2.3) have found that  $t_0 = 2.12 \cdot 10^{-16}$  sec in the energy region of interest. The difference between  $f_0$  and  $F$  is that  $f_0$  is the neutral fraction following a passage through a thick foil,  $F_H$  and  $F_p$  are valid even for very thin foils where charge equilibration does not occur. It can be verified directly from eqs. (2.7) and (2.8) that in the limit of long dwell times  $F_H = F_p = f_0$ , as required.

The electron transmission through a foil is assumed to be described by the expression

$$P_e(x,V) = \exp(-x/L_{eff}(V)) \quad (2.9)$$

where  $L_{eff}$  is electron effective mean free path in the foil. The instrument will detect electrons that have suffered some angular scattering and energy straggling so that  $L_{eff}$  can be considerably larger than the mean free path for inelastic scattering,  $L_0$ . In the energy region of interest, the mean free electron path has been observed to increase approximately linearly with velocity (Ref. 2.3). Thus we can write

$$L_{eff}(V) = K_{eff} \cdot V . \quad (2.10)$$

The probability that a neutral hydrogen atom will suffer an ionizing collision after a distance  $x$  in the foil is

$$C(x,V) = 1 - \exp\{-\sigma_i(V) \cdot Nx\} . \quad (2.11)$$

This expression ignores the contribution from multiple stripping and pickup processes. This is justified by the fact that these processes are not important since  $\sigma_i \gg \sigma_c$ . In a section of foil of thickness  $dx$ , the differential ionization probability is given by

$$dC(x,V) = \sigma_i(V) \cdot N \cdot dx = \sigma_i(V) \cdot N \cdot V \cdot dt \quad (2.12)$$

Eq. (2.6) can be solved analytically using the functional forms given in eqs. (2.7), (2.8), (2.9), (2.11) and (2.12). The solution for incident protons is

$$Ne_p = \frac{f_0}{t_0} [\mu^{-1}(1 - \exp(-\mu t_d)) - \alpha(\exp(-t_d/t_0) - \exp(-\mu t_d))] \quad (2.13)$$

while for incident neutral atomic hydrogen it is

$$Ne_H = \frac{f_0}{t_0 \mu} [1 - \exp(-\mu t_d)] + \frac{\alpha}{t_0} (\exp(-t_d/t_0) - \exp(-\mu t_d)) \quad (2.14)$$

where  $\mu = V/L_{eff}(V) = 1/K_{eff}$  and  $\alpha = t_0/(t_0 \mu - 1)$ . Convoy electron production rates, calculated using eqs. (2.13) and (2.14), for 2

and  $5 \mu\text{g}/\text{cm}^2$  carbon stripper foils are plotted in Figure 2.2. The constant  $\mu$  was set to  $7.5 \cdot 10^{15} \text{ sec}^{-1}$ , a value measured for 932 eV electrons by Latz et al. (Ref 2.5). Convoy electron energy of 932 eV corresponds to a proton beam energy of 1.7 MeV.

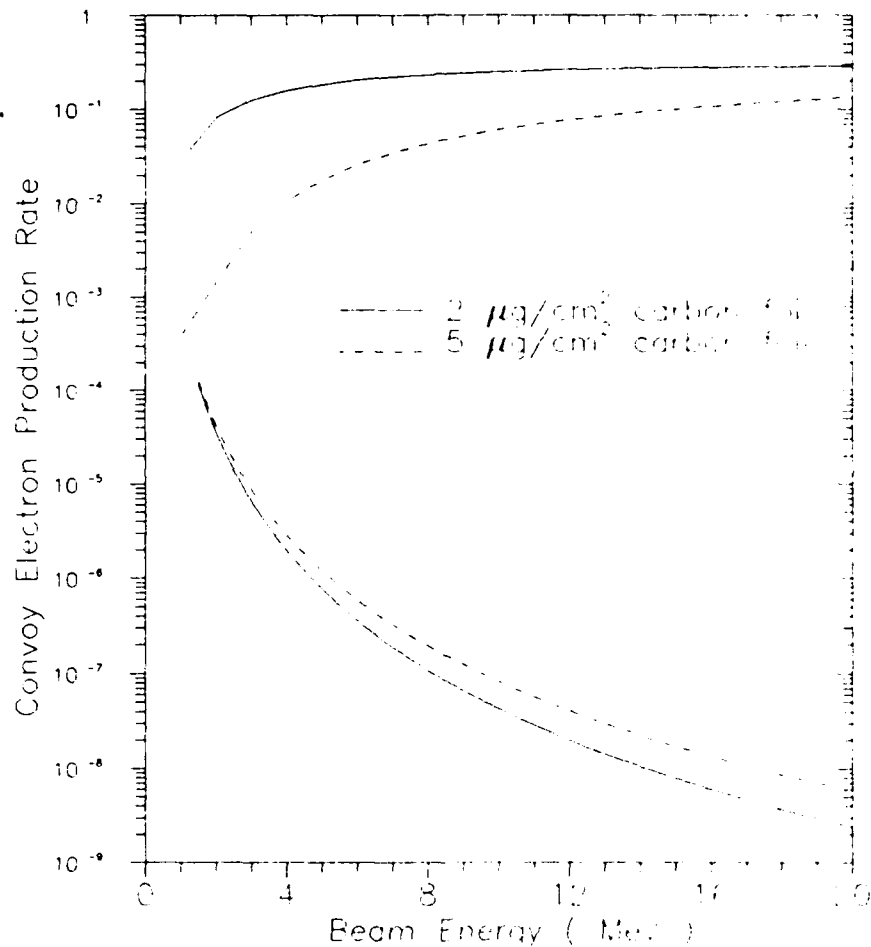


Figure 2.2 Calculated convoy electron production rates per incident beam particle. Top two curves correspond to incident neutral particles, the bottom two to charged ones.



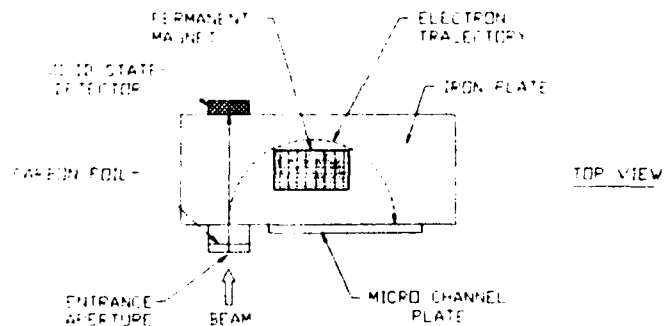
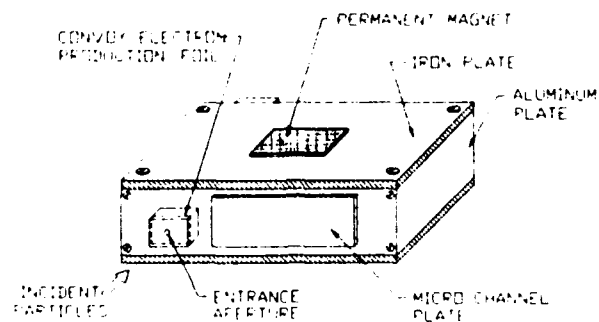


Figure 3.1 Schematic diagram of the magnetic analyzer instrument.

### 3. EXPERIMENTAL EQUIPMENT

#### 3.1 Magnetic Analyzer Breadboard Instrument

The initial version of the breadboard instrument, to be used in the testing of the concept of neutral particle detection using accelerator beams, was a  $180^\circ$  magnetic electron energy analyzer. The mechanical construction of the detector is shown in Fig. 3.1. Incident beam particles (protons or neutral hydrogen atoms)

traverse the thin carbon foil,  $2 - 5 \mu\text{g}/\text{cm}^2$  areal density, move essentially without deflection through the magnetic spectrometer and are detected in the solid state detector (SSD). The forward going electrons, produced by the passage of the beam particles through the foil, enter the spectrometer. Their trajectories are bent by the magnetic field and the electrons impact on the 5 cm long and 0.8 cm high MCP, which is mounted in the focal plane of the spectrometer. The MCP has a resistive, position-sensitive anode so that the location of the crossing of the focal plane by the electron trajectory or, equivalently, its velocity can be determined. The geometry of the spectrometer and the applied magnetic field is such that only electrons with energies greater than 0.5 keV will be detected in the MCP.

The magnetic field of the spectrometer is provided by permanent NdFe magnets mounted on two 2" by 5" iron plates, separated by 1.5" aluminum spacers. The magnetic field is roughly perpendicular to the iron plates and its strength can be set to approximately 50 gauss by placing one magnet or 110 gauss by placing two magnets on each plate. The magnetic fields in both configurations have been carefully mapped out using a magnetometer. In particular, care was taken to measure the fringe fields and non-perpendicular magnetic field components so that a realistic calculation of electron trajectories could be performed.

The magnetic breadboard instrument has a single  $200 \text{ mm}^2$  solid state detector, located behind the spectrometer, to detect beam particles coincident with electrons detected in the MCP. A flight instrument would need two such detectors arranged as a E-dE telescope. A telescope will be necessary because in orbit, unlike in an accelerator experiment, the identity of incoming particles is not known and the telescope energy loss information can be used to deduce the identity of the bombarding particles.

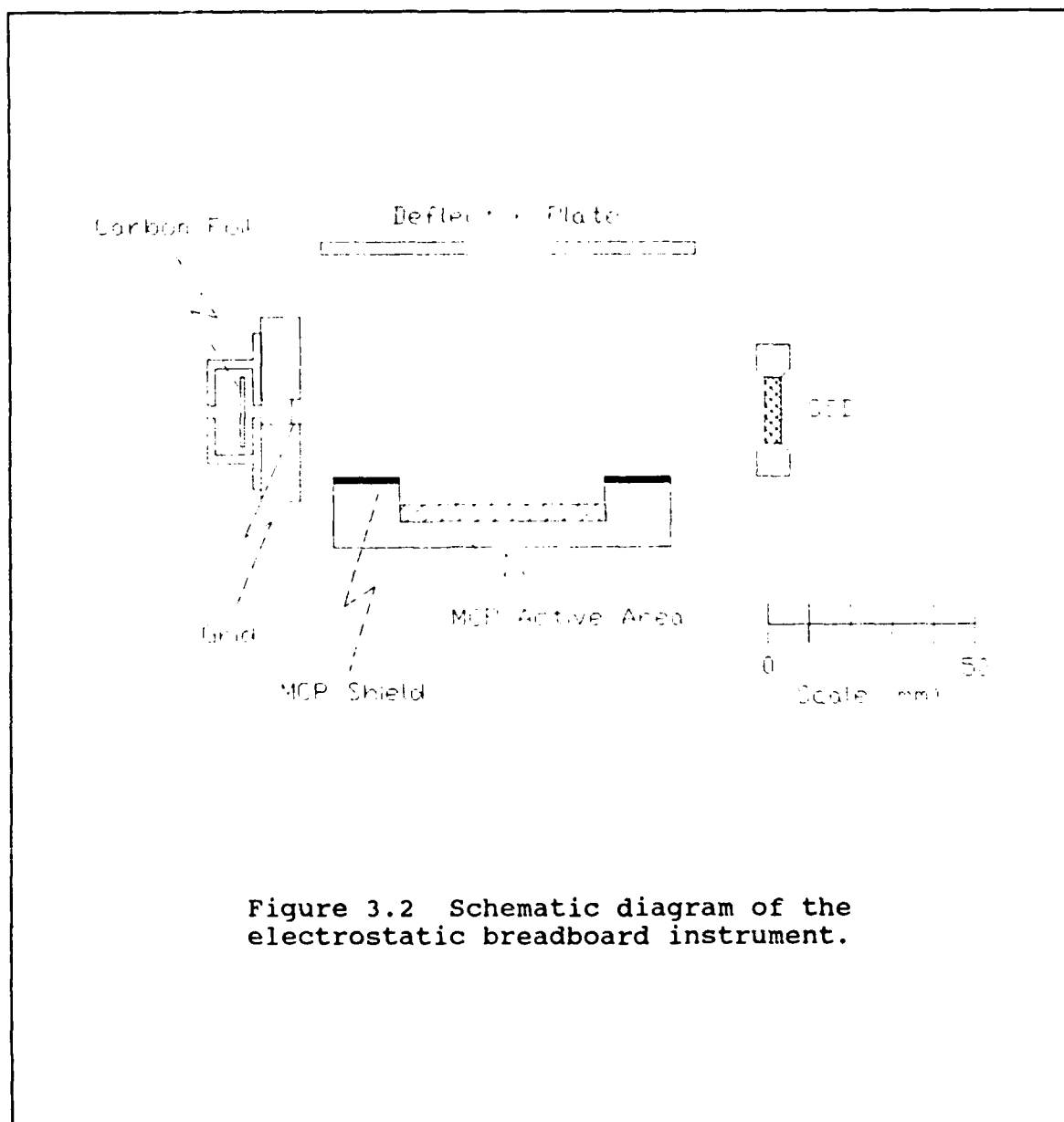


Figure 3.2 Schematic diagram of the electrostatic breadboard instrument.

### 3.2 Electrostatic Breadboard Instrument

The final configuration of the breadboard instrument, based on the work with the magnetic analyzer, used an electric field, instead of a magnetic one, to deflect the convoy electrons onto the MCP. A schematic of the instrument is shown in Figure 3.2.

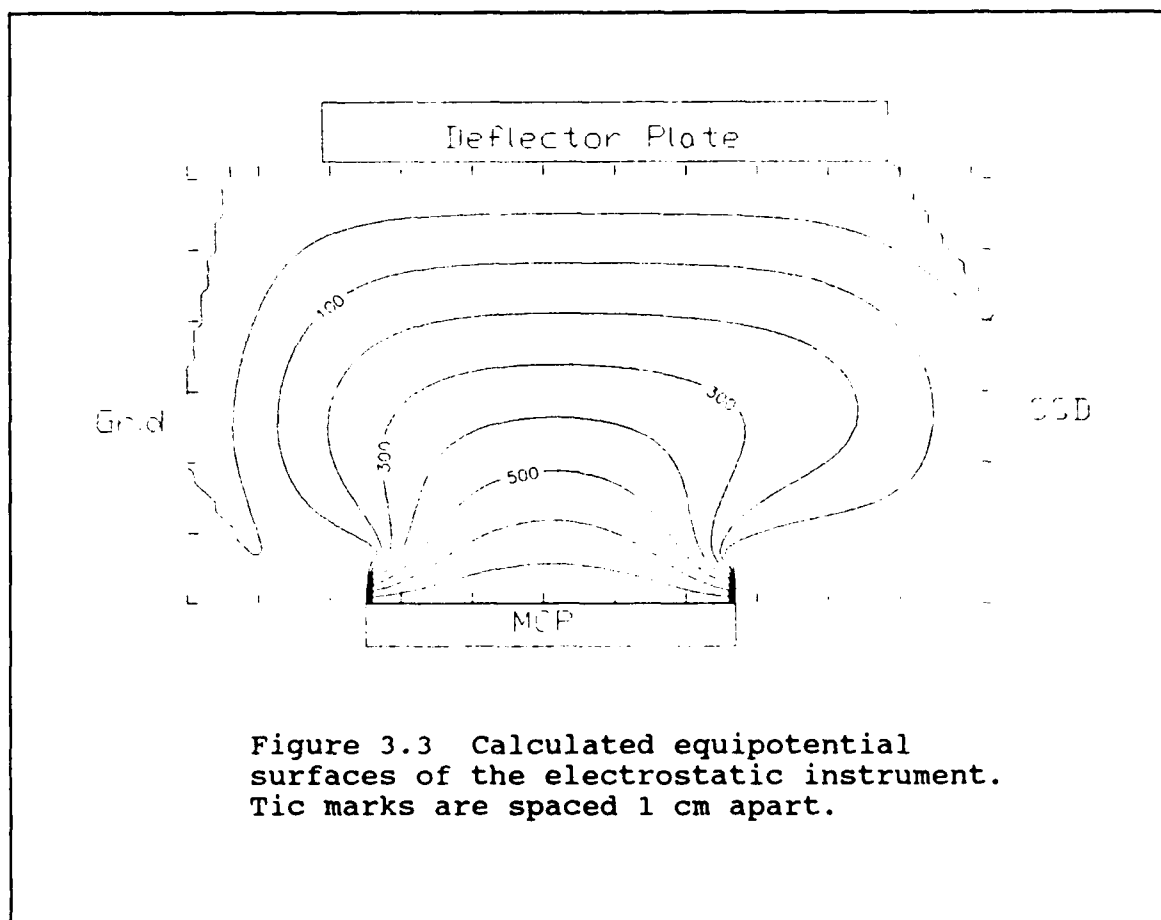


Figure 3.3 Calculated equipotential surfaces of the electrostatic instrument. Tic marks are spaced 1 cm apart.

The incident beam is made to traverse the thin carbon foil at the entrance to the instrument. The protons that emerge from the foil travel without significant deflection through the instrument and are detected by the solid state detector. The forward moving electrons with energy sufficient to overcome the grid voltage bias enter the gap between the deflector plate and the MCP are swept to the MCP by the applied electric field. The field is generated by applying a negative voltage to the deflector plate and a high positive voltage to the front of the MCP. The nominal voltages used during the experiments were  $V_{\text{grid}} = -100 \text{ V}$ ,  $V_{\text{MCP}} = +800 \text{ V}$ ,  $V_{\text{plate}} = -100 \text{ V}$ . All other metallic surfaces, including the MCP shield plate which surrounded the active opening area of the MCP, were held at ground potential.

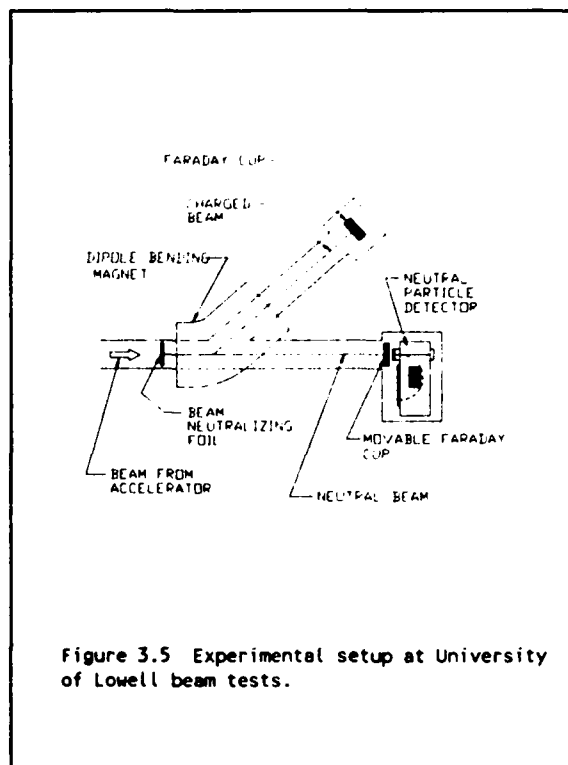
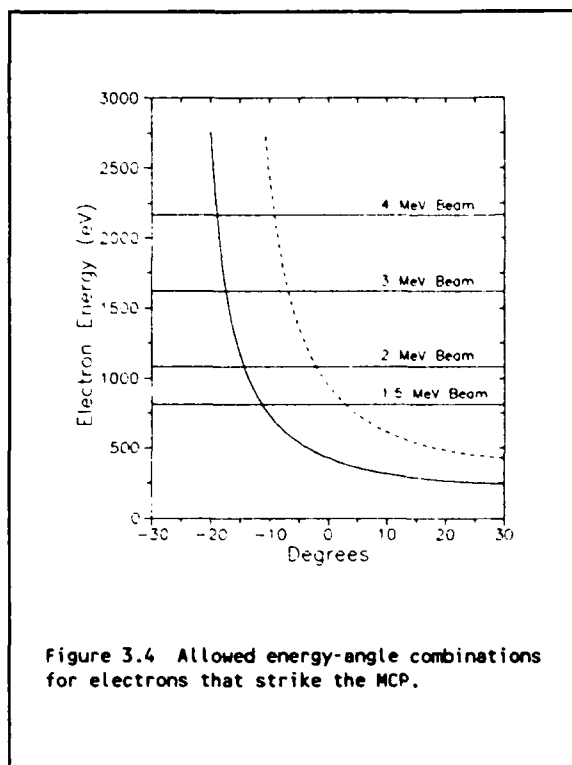
The electric potential surfaces in the center plane of the instrument are shown plotted in Figure 3.3. The surfaces were

calculated by numerically solving Laplace's equation for the electric potential for the geometry of the instrument, using the nominal values of the voltages. Since the electric field lines are orthogonal to the equipotential surfaces it is evident from Figure 3.3 that all electric field lines that start on the grid must end on the right side of the MCP, lines that begin on the SSD end on the left side of the MCP and the lines that start on the deflector plate end in the center section of the MCP. Results of calculations show that the grid electric field lines are confined to the left most 1.7 cm of the MCP, the deflector plate lines the next 1.6 cm and the SSD lines to the right most 1.7 cm. This feature of the electric field lines will be used in Section 4 to interpret the collected data.

The knowledge of trajectories of electrons emitted from the foil as a function of energy and angle of emission is necessary for the analysis of the data. Electron trajectories can be considered in the following way. Electrons coming out of the foil with low energies, typically a few eV, are confined to motion along the electric field lines and, therefore, all strike the left side of the MCP. Higher energy electrons are not strongly affected by the electric field near the grid, but instead spend most time in the deflector plate - MCP gap where the electric field is nearly constant and perpendicular to the beam axis. Motion of electrons in such a field is described by

$$y(x) = \frac{-eE_0x^2}{4T \cdot \cos^2\theta} + x \cdot \tan\theta + y_0 \quad (3.1)$$

Equation (3.1) is a solution of the equation of motion for a charged particle in a uniform electric field. The coordinate system is defined such that the X axis lies parallel to and along the front of the MCP and the Y axis lies parallel to and along the carbon foil. T is the electron kinetic energy in keV, e is the electron charge,  $E_0$  is the applied electric field in V/cm,  $y_0$  is the distance along the Y axis from the origin to the center of the foil and  $\theta$  is the angle of emission with respect to the beam axis. Equation (3.1) can be solved to yield the values of T and  $\theta$  for which the electron will strike the MCP. The allowed values are



shown in Figure 3.4. All electrons with  $T$  and  $\theta$  values below the dashed curve will hit somewhere on the MCP, while those with values under the solid curve will hit to the left of MCP center. The horizontal lines show the electron energy of beam velocity electrons for the various beam energies used during the experiments.

### 3.3 Accelerator Test Setup

Neutral and charged beams are necessary for testing and calibration of the instrument. Charged beams are easily obtained from Van de Graaff accelerators. However, generation of neutral beams poses a significant challenge. The accelerator arrangement used during the tests at University of Lowell Van de Graaff is shown in Fig. 3.5.

A charged proton beam from a Van de Graaff is made to traverse a 0.15 mil thick Al beam neutralizing foil. Some of the beam

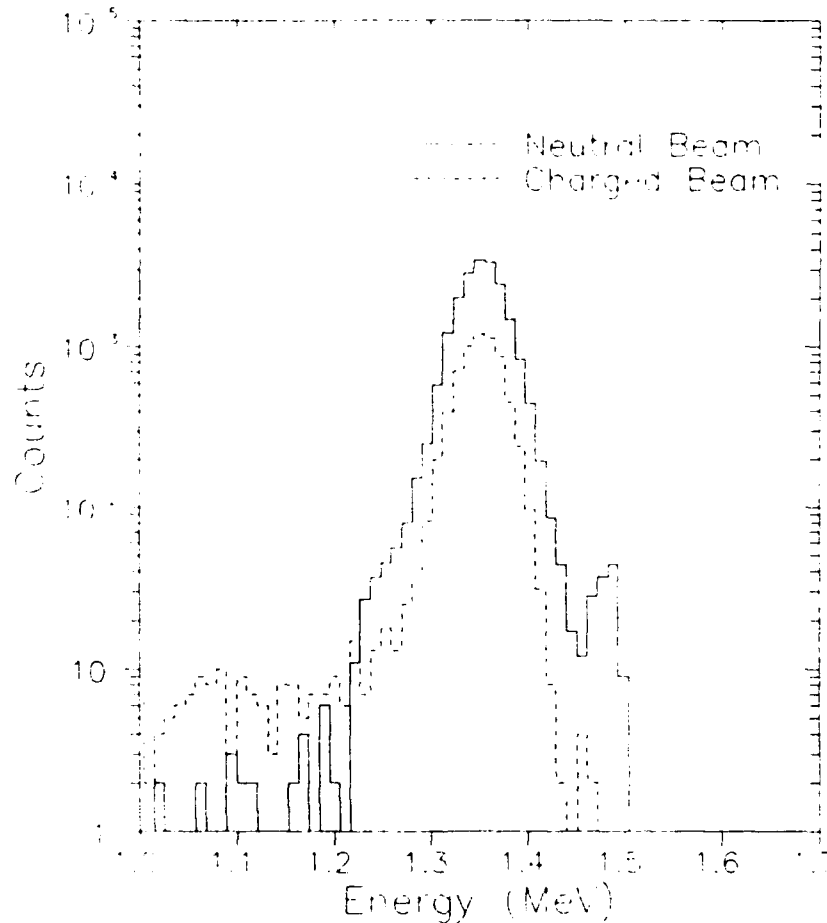


Figure 3.6 Beam energy profiles as measured by the solid state detector for a 1.5 MeV beam.

particles pick up an electron from the foil and become neutral hydrogen atoms. The dipole magnet, located downstream of the foil, bends the charged fraction of the beam to a chamber where the beam intensity can be monitored. The neutral beam particles continue undeflected through the magnet and exit through the  $0^\circ$  port into the breadboard instrument. If the response of the instrument to charged particles is desired, the beam-neutralizing Al foil is removed and the dipole magnet is switched off so that the charged beam exits through the  $0^\circ$  port.

Energy profiles of 1.5 MeV neutral and charged beams, as measured by the SSD in the instrument are shown in Figure 3.6. It

is evident that the neutral beam has two energy peaks separated by approximately 140 keV. The lower energy peak has a FWHM of 54 keV while the high energy peak, with a strength of 0.1 to 1% of the low energy peak, has a FWHM of less than 20 keV, approximately equal to the SSD resolution. The charged beam lacks the high energy component.

The observed structure in the beam profiles can be understood in the following way. The proton beam travels vertically down from the exit of the Van de Graaff accelerator and is momentum analyzed by a 90° analyzing magnet. After the analyzing magnet there is a 25 foot drift section before the neutralizing foil. Some beam protons undergo charge exchange collisions with the residual gas atoms in the drift section and become neutral hydrogen atoms, moving with beam velocity. A small fraction of the foil area consists of microscopic pin holes and beam particles traveling through them do not suffer any scattering. When the dipole bending magnet is turned on, the particles striking the SSD are either beam protons that were neutralized in the foil, and suffered energy losses and energy and angular straggling, or neutral beam velocity hydrogen atoms that travelled through the pin holes and have not been scattered in the foil.

The second group of detected particles should be much less numerous than the first because the foil area covered by pin holes is small. Therefore, the SSD energy distribution would have a large peak at a lower energy and a small, much narrower peak at a higher energy, with the two peaks separated by approximately 130 keV (energy loss of 1.5 MeV protons in 0.15 mils of Al). This is precisely what is evidenced by data shown in Figure 3.6. The separation of the two peaks should decrease with increasing beam energy, as the slower particles have a larger rate of energy loss than the faster ones. The observed and calculated peak separations are shown in Table 3.1. There is good agreement between data and calculations.

The absence of the high energy peak in the charged beam spectrum is probably due to the method of steering the charged beam into the instrument. The charged beam is so intense that it must be highly defocused and steered slightly off the nominal beam axis in order to produce an acceptable count rate in the SSD. As a



result, the beam particles strike the neutralizing foil at a slight oblique angle. The diameter of the microscopic pin holes is much smaller than their length and, therefore, no trajectories of particles that hit the SSD can be contained completely inside the pin holes. Consequently, all detected beam particles suffer some energy loss.

#### 4. EXPERIMENTAL RESULTS AND DATA ANALYSIS

##### 4.1 Magnetic Device - Experimental Results

The initial experiments at the University of Lowell accelerator were done using the magnetic analyzer version of the

---

Table 3.1

Calculated and measured energy separation between beam particles that traverse the foil and those that travel through the pinholes in the foil.

E (MeV)	Calculated $\delta E$ (keV)	Measured $\delta E$ (keV)
1.5	127	138
2.0	114	101
3.0	86	74
4.0	70	64

instrument. Early efforts were plagued by the difficulties of obtaining neutral beams and maintaining beam stability with beam currents orders of magnitude below the normal operating currents of the Lowell Van de Graaff. The data collected after the accelerator problems were solved showed no difference between charged and neutral beams. The MCP-SSD coincidence yields were at a level consistent with accidental coincidences between beam protons and background radiation particles capable of triggering the MCP (i.e. electrons, alpha particles, protons and UV and X-ray photons).

The probable cause of failure to detect convoy electrons was the inhomogeneity of the magnetic field of the analyzer which greatly reduced the electron detection efficiency of the instrument. The ideal magnetic field in the parallel plate geometry is perpendicular to the planes of the plates and constant in magnitude. The field actually achieved in the analyzer was only an approximation to the ideal field. Magnetometer measurements showed that the B field components parallel to the plates were of the order of 10% of the perpendicular field in the center of the analyzer and much larger near the edges of the plates. The effect of the parallel field components is to shift the electron trajectories vertically out of the focal plane. The vertical extent of the MCP is only 0.4 cm on either side of the focal plane so that most of the electron trajectories may have missed the MCP.

#### 4.2 Electrostatic Device - Experimental Results

Results of experiments performed with the electrostatic version of the instrument showed that the instrument is capable of detecting convoy electrons produced by proton and neutral hydrogen beams and that is capable of distinguishing between neutral and charged beams. Experimental work was done using charged and neutral beams with energies between 1.5 and 4.0 MeV and carbon foils with thickness of 2, 5 and 10  $\mu\text{g}/\text{cm}^2$ . Table 4.1 contains the listing of beam energies and foil thicknesses studied. The evidence for convoy electron detection is described in sections

4.2.1 and 4.2.2 while section 4.2.3 contains information about another possible way of distinguishing neutral and charged beams.

#### 4.2.1 MCP Position Spectra

A typical singles MCP position spectrum, taken during a run with a neutral 4 MeV beam, is shown in Figure 4.1. The most evident feature of the data, the two position peaks, can be directly explained by consideration of the electric field configuration inside the instrument. The bulk of electrons produced by the interaction of fast beam particles with matter are very low in energy, typically a few eV, and convoy electrons are a small fraction of the total electron yield. These low energy electrons, produced at the foil and at the SSD front surface, are confined to move along electric field lines. Therefore, as was demonstrated in Section 3.2, electrons produced at the foil will strike the MCP at the front edge, those produced at the SSD will

---

Table 4.1

Listing of beam energies and foils used during experiments.

Beam Energy (MeV)	Foil Areal Density ( $\mu\text{g}/\text{cm}^2$ )
1.5	5
2.0	2, 5, none
3.0	2, 5, none
4.0	2, 5, 10, none

---

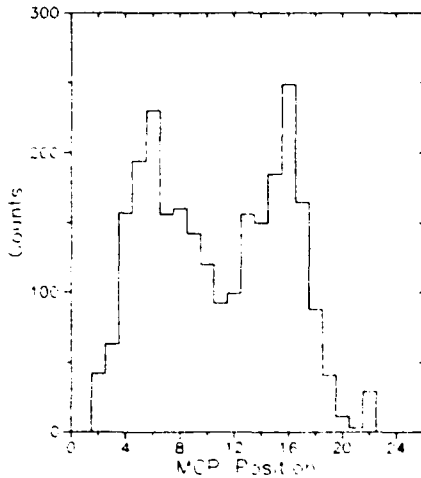


Figure 4.1 Singles MCP spectrum:  
neutral beam, 4 MeV beam energy.  
Foil areal density:  $5 \mu\text{g}/\text{cm}^2$ .

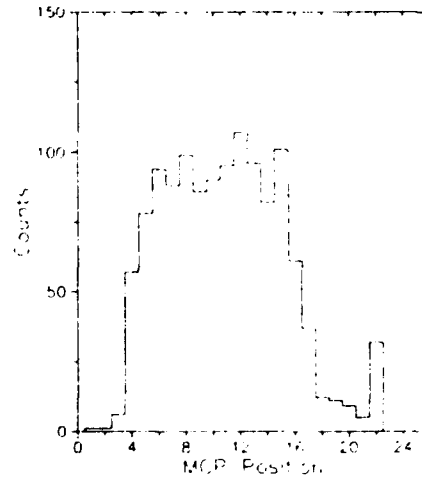


Figure 4.2 Coincidence MCP spectrum:  
neutral beam, 4 MeV beam energy.  
Foil areal density:  $5 \mu\text{g}/\text{cm}^2$ .

hit the back edge and none will hit the central third on the MCP. The spectrum shown in Figure 4.1 agrees very well with the theoretically predicted spectrum. The counts in the middle third of the observed spectrum are due to finite MCP resolution, higher energy electrons not confined to electric field lines and photons. Singles MCP position spectra obtained during runs with charged beams are very similar to those from neutral beam runs with the only difference being that at 1.5 and 2.0 MeV the front peak in the MCP position spectrum is larger than the back peak.

MCP position spectra taken in coincidence with a beam particle detected by the SSD are very different in nature than the singles spectra. The neutral beam position spectra (see Figure 4.2) are flat across the MCP aperture. This is the expected position spectrum distribution of convoy electrons, since their high kinetic energy and angular spread at exit from the foil enables them to reach all parts of the MCP (see Figure 3.4). The charged beam position spectra (Figure 4.3) are much flatter than the singles spectra but all show some evidence for forward peaking, indicating that low energy electrons from the foil are an important part of the charged beam electron yield.

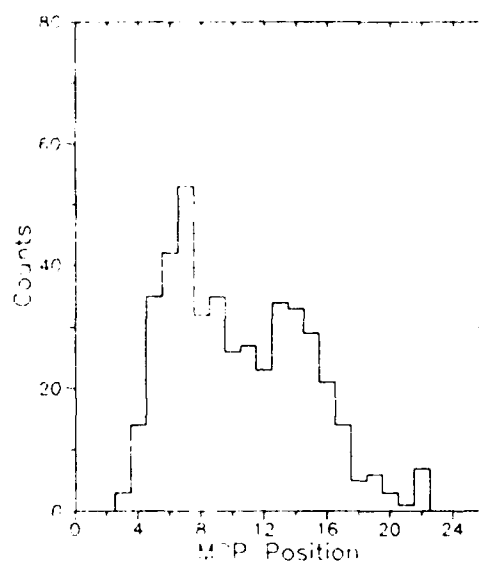


Figure 4.3 Coincidence MCP spectrum:  
charged beam, 4 MeV beam energy.  
foil areal density:  $5 \mu\text{g}/\text{cm}^2$ .

#### 4.2.2 Experimental and Calculated Electron Yields

Measured yields of electrons in coincidence with beam particles are listed in Table 4.2. The SSD-MCP coincidence counts, electrons associated with beam protons, were normalized to the total number of singles SSD counts, effectively the beam intensity. A small correction, typically 10%, for accidental coincidences is included in the tabulated values.

It is evident that there is a substantial increase in yield going from charged to neutral beams and that difference increases with beam energy. Furthermore, the electron yield increases as the foil thickness decreases. All the above observations are consistent with the dominant mode of convoy electron production, stripping the electron from the beam projectile at the front of the stripper foil. The electron suffers scattering as it traverses the

foil and the thicker the foil the more scattering it undergoes. Consequently, thick foils produce more electron loss than thin ones and convoy electron yield decreases with increasing foil thickness.

The cleanest comparison between the simple model of convoy electron production from Section 2 and the data is the calculated and measured difference in electron yield between neutral and charged beams. Accordingly an experimental quantity  $\delta R = R_n - R_c$

Table 4.2

Electron yields measured with the electrostatic instrument. Indicated errors are statistical only. Yields are corrected for accidental SSD-MCP coincidences.

Energy (MeV)	Foil ( $\mu\text{g}/\text{sq.cm}$ )	R (x1,000) Neutral Beam	R (x1,000) Charged Beam	$\delta R$ (x1,000)
1.5	5	$7.2 \pm 0.2$	$6.4 \pm 0.2$	$0.8 \pm 0.3$
2.0	2	$9.6 \pm 0.3$	$5.3 \pm 0.3$	$4.3 \pm 0.4$
2.0	5	$6.8 \pm 0.2$	$5.5 \pm 0.2$	$1.3 \pm 0.3$
3.0	2	$15.2 \pm 0.4$	$4.2 \pm 0.2$	$11.0 \pm 0.5$
3.0	5	$7.7 \pm 0.2$	$4.7 \pm 0.2$	$3.0 \pm 0.3$
4.0	2	$17.1 \pm 0.6$	$3.4 \pm 0.4$	$13.7 \pm 0.7$
4.0	5	$10.3 \pm 0.3$	$4.0 \pm 0.2$	$6.3 \pm 0.4$
4.0	10	$7.8 \pm 0.4$	$3.8 \pm 0.3$	$4.0 \pm 0.5$

$R = \text{SSD-MCP Coincidence Counts} / \text{SSD Singles Counts}$

$\delta R = R_{\text{Neutral}} - R_{\text{Charged}}$

was defined, where  $R$  is the coincidence electron yield and the subscripts  $n$  and  $c$  denote the neutral and charged beams. Experimental values of  $\delta R$  are listed in Table 4.2. Calculating the difference of the two yields, eliminates any background processes, such as X-ray emission stimulated by the beam particle's passage through the foil, which can also give rise to MCP-SSD coincidences.

The theoretical values of  $\delta R$  were calculated using  $\delta R = \epsilon (Ne_n - Ne_p)$  where  $Ne_n$  and  $Ne_p$  are obtained from eqs. (2.13) and (2.14) and  $\epsilon$  is an approximation for the efficiency of the MCP for detecting convoy electrons. The adjustable factor  $\epsilon$  includes both the effects of the intrinsic MCP electron detection efficiency, approximately 80%, and the finite size of the MCP detector. Although the horizontal extent of the MCP is 5 cm, its vertical coverage is only 0.8 cm. The typical electron flight path length is of the order of 6 cm and, therefore, electrons emitted with vertical angles larger than about  $4^\circ$  will miss the MCP. The only other adjustable parameter is  $K_{eff}$ , which determines the effective electron mean free path.

Results of calculations, with  $\epsilon = 0.045$  and  $K_{eff}$  corresponding to  $L_{eff} = 58.1 \text{ \AA}$  for 932 eV electrons, are in good agreement with the data for both 2 and 5  $\mu\text{g}/\text{cm}^2$  foils (Figure 4.4). Solid line shows the calculated values while the dashed lines show the effects of including the uncertainties in carbon foil density and foil thickness. Doubling the  $L_{eff}$  value (Figure 4.5) reduces the quality of the fit to the data. The calculated curves, especially for the 2  $\mu\text{g}/\text{cm}^2$  foil, show a slightly different trend than the data. Decreasing the  $L_{eff}$  value to 40  $\text{\AA}$  (Figure 4.6) also degrades the fit, in this case the calculation cannot simultaneously reproduce the magnitude of data for the 2 and 5  $\mu\text{g}/\text{cm}^2$  foils. It should be noted that the shape of the calculated curves is affected only by  $L_{eff}$ ,  $\epsilon$  simply shifts the curves vertically on the logarithmic plot.

The extracted value of  $L_{eff}$  for 932 eV electrons, approximately 60  $\text{\AA}$ , is a reasonable one for this experiment. The mean free path for electron inelastic scattering at this energy is characterized by a  $L_0 = 15.8 \text{ \AA}$  (Ref 2.4). Latz *et al.* (Ref 2.5) measured

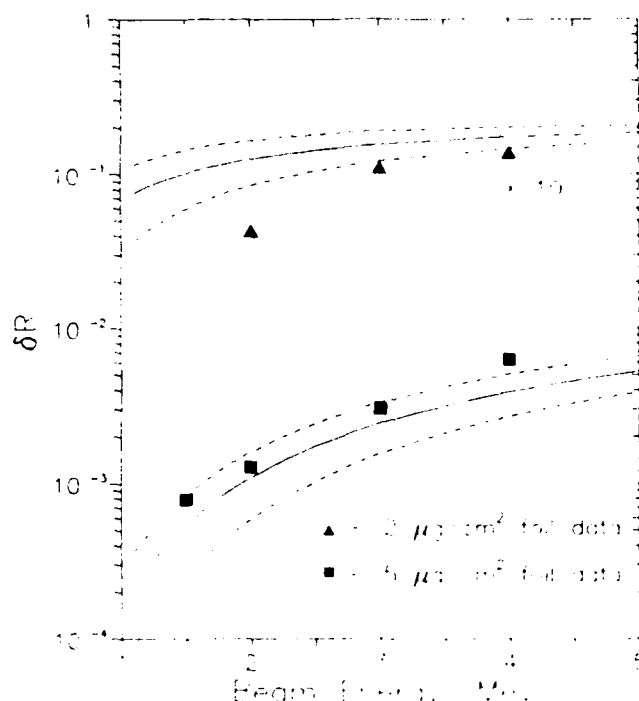


Figure 4.4 Measured and calculated values of  $\delta R$ . Calculation parameters:  $\epsilon = 0.045$ ,  $L_{\text{eff}} = 58 \text{ \AA}$ .  $2 \mu\text{g}/\text{cm}^2$  foil data and calculated curves are multiplied by 10.

$L_{\text{eff}} = 24.3 \text{ \AA}$  in a geometry that allowed for a small amount of angular and energy scattering. In this experiment, as is evident from examination of Figure 3.4, a large amount of electron angular scattering and energy straggling was allowed. Therefore, the measured effective electron mean free path should be larger than the inelastic scattering mean free path and the mean free path measured by Latz et al.

#### 4.2.3 Electron Yields Without Stripper Foil

In addition to beam tests with 2 and 5  $\mu\text{g}/\text{cm}^2$  foils, measurements were also performed with the carbon stripper foil



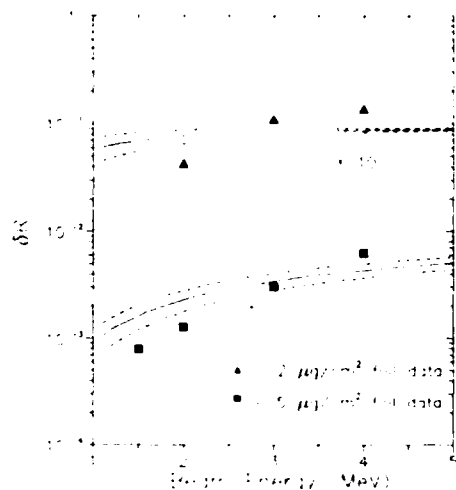


Figure 4.5 Measured and calculated values of  $\delta R$ . Calculation parameters:  $\epsilon = 0.015$ ,  $L_{\text{eff}} = 121 \text{ \AA}$ .  $2 \mu\text{g}/\text{cm}^2$  foil data and calculated curves are multiplied by 10.

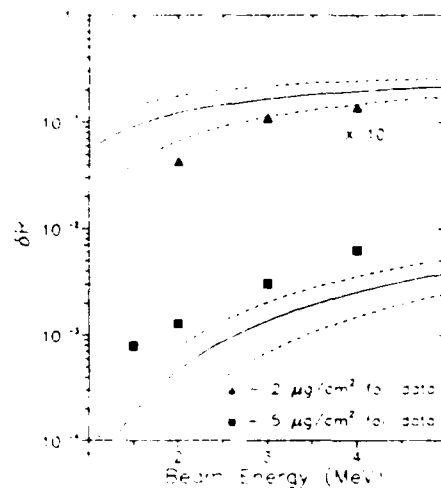


Figure 4.6 Measured and calculated values of  $\delta R$ . Calculation parameters:  $\epsilon = 0.070$ ,  $L_{\text{eff}} = 40 \text{ \AA}$ .  $2 \mu\text{g}/\text{cm}^2$  foil data and calculated curves are multiplied by 10.

removed. Coincidence electron yields for charged beams were lower than for runs with a stripper foil in place but the neutral beam yields were higher, significantly higher for the lowest energy. The measured coincidence rates are listed in Table 4.3.

The source of the electrons responsible for the surprisingly high yields for neutral beams can be identified from the MCP position spectra taken during the experiment. Neutral beam MCP spectra (see Figure 4.7) have a small peak at the front of the MCP and a larger one at the back. Charged beam spectra (see Figure 4.8) have only the forward peak. Beam scattering from the entrance aperture will produce low energy electrons which will strike the front of the MCP, thus accounting for the forward peak. The backward position peak, which occurs in the neutral beam MCP

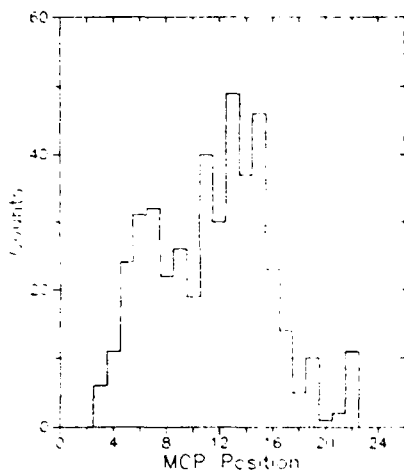


Figure 4.7 Coincidence MCP position spectrum:  
Neutral beam, 4 MeV beam energy, no carbon foil.

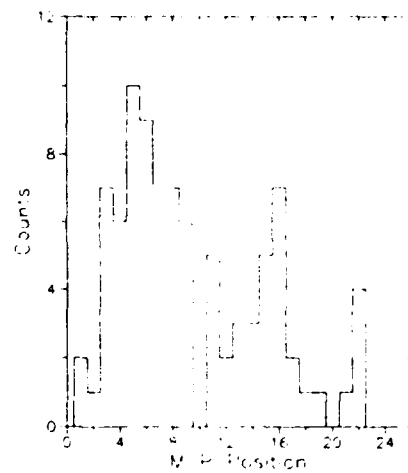


Figure 4.8 Coincidence MCP position spectrum:  
charged beam, 4 MeV beam energy, no carbon foil.

Table 4.3

Summary of results obtained with no stripping foil.

Beam Energy (MeV)	Neutral or Charged	R (x1,000)
2.0	N	17.9
2.0	C	4.4
3.0	N	21.0
4.0	N	20.8
4.0	C	1.9

spectra only, is most likely due to stripping of the electron from the neutral hydrogen projectile in the first few atomic layers of the SSD and the subsequent back scattering of stripped electrons. Kinematics of collisions leading to back scattering will leave the electron with very low kinetic energy and, even though the back scattering probability is small, the electric fields in the instrument (Figure 3.3) will ensure very efficient transport to the MCP.

#### 4.3 Summary of Results

Data taken with electrostatic field version of the instrument, described in Section 3.2, show that the coincidence electron yields are significantly different for charged and neutral beams. Measured count rates and position spectra can be understood within the framework of the simple convoy electron production model outlined in Section 2. The coincidence yields observed with the stripper foil removed can be accounted for by the process of back scattering of electrons stripped from the projectile in the solid state detector. In fact, these backscattered electrons provide a second method for distinguishing charged and neutral beams.

#### 5. PRELIMINARY ENGINEERING MODEL DESIGN

As a result of the experimental work described above, two related instrument designs are proposed for the engineering model of the flight instrument. The proposed instruments are similar enough so that they could be constructed and tested with little additional effort above that needed for a single design. Instrument beam tests could be carried out at the University of Lowell facility for beam energies below 4.5 MeV and at the Yale University ESTU Van de Graaff facility for beam energies up to 40 MeV.

## 5.1 Mechanical Design

Use of the MCP as the electron detector was a result of the historical progress of the work on this contract and the availability of equipment. The MCP turned out to be valuable in the research phase of this effort because the electron position spectra were useful in understanding the physics under study as well as the properties of the instrument. For the engineering model and the flight instrument, however, channeltrons are a better choice for the electron detector than the MCP. They are simpler to read out, less susceptible to environmental damage, less expensive and have a much longer, and very good, space flight history.

The schematic design of version A of the engineering model is shown in Figure 5.1. This version of the instrument is identical in principle to the breadboard instrument except that channeltrons replace the MCP as the electron detector. The collimator and carbon foil would be held at a ground potential. Grid #1 would be at a voltage of about -100 V to stop very low energy electrons that are copiously produced by beam-foil interactions. The funnel of the channeltron would be at a high positive voltage, of the order of a few kV, to attract most electrons that travelled through the grid. The electric field between grid #1 and the channeltron funnels would be further shaped by the electric field guard ring and grid #2. Both would be held at a negative voltage of the order of -500 V to increase the efficiency of convoy electron collection. In addition, grid #2 would prevent low energy electrons emitted from the Al foil in front of the SSD's from reaching the funnels. Beam particles would be detected in the solid state detector telescope. The magnets on the collimator snout are there to deflect away, from the entrance aperture of the instrument, the large flux of very low energy protons and electrons found in the radiation belts. An Al or Ni foil just in front of the SSD is required for additional detector shielding, particularly from light. Without sufficient shielding a detector may be saturated and driven inoperable by intense low energy particle or light fluxes.

Version B of the engineering model (see Figure 5.2) takes advantage of the effect of stripping and back scattering of electrons from neutral projectiles, as described in Section 4.2.3. There is no need for a stripper carbon foil and the channeltrons are pointed at the SSD. The Al or Ni foil in front of the SSD serves the dual purpose of light shielding the SSD and of stripping and back scattering electrons from fast neutral hydrogen atoms. The foil and the SSD would be at ground potential while the channeltron funnels would be set at a high positive voltage to attract the backscattered electrons. The electric field between the Al foil and the channeltron funnels would be further shaped by the electric field guard ring and the grid. Both would be held at a negative voltage of the order of -500 V to increase the efficiency of convoy electron collection. A second grid, located between the foil and the field guard ring, and held a voltage of -5 to -10 V, may be useful in shielding the channeltrons from very low energy photoelectrons ejected from the foil by incident ultraviolet light. However, since the backscattered electrons may be low in energy, the second grid may result in significantly

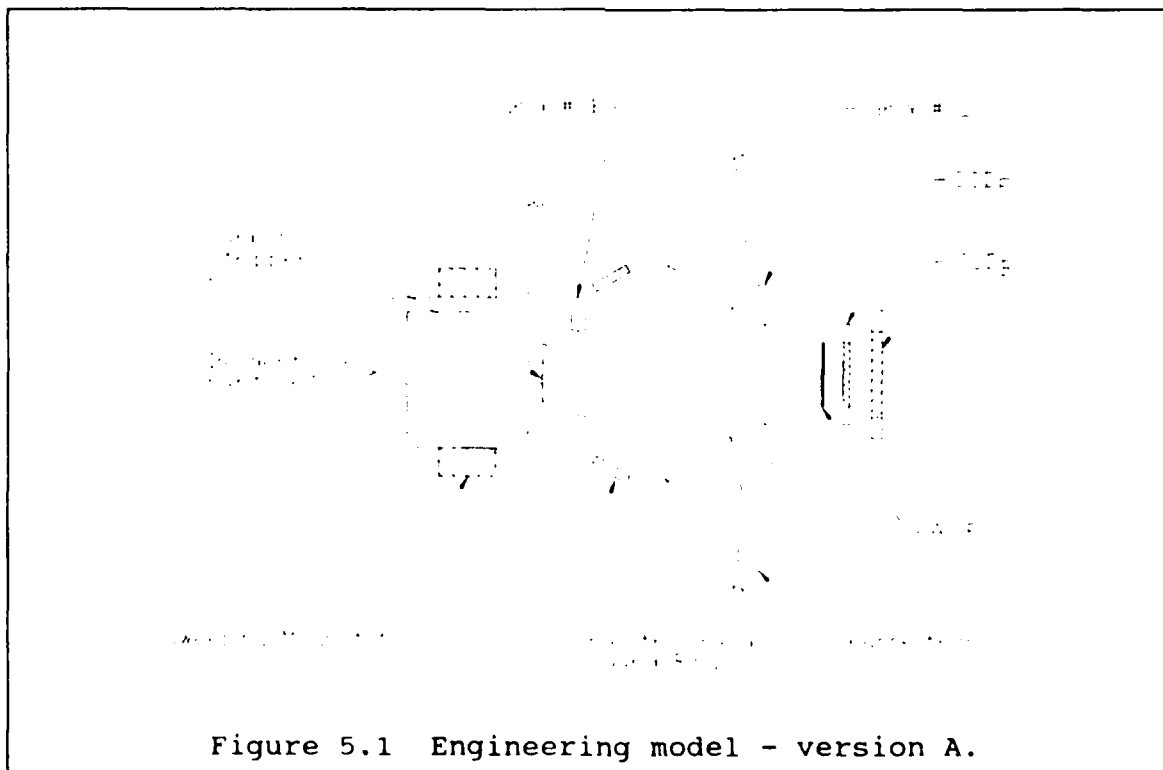


Figure 5.1 Engineering model - version A.

reduced yields from neutral particles, and its use will depend on measurements made with the engineering model unit.

One advantage of version B over version A is that there is no need for the thin,  $2 - 5 \mu\text{g}/\text{cm}^2$ , carbon stripper foil. Although such foils have been successfully flown on spacecraft, they are delicate and subject to degradation under the bombardment of the high particle flux in the radiation belts. However, both designs must still be evaluated for their ability to distinguish neutral hydrogen from protons in the laboratory and in the space environment. The improvements in the designs of the engineering models over the breadboard model leave an open question as to which of the two is the superior instrument for a given incident particle energy range.

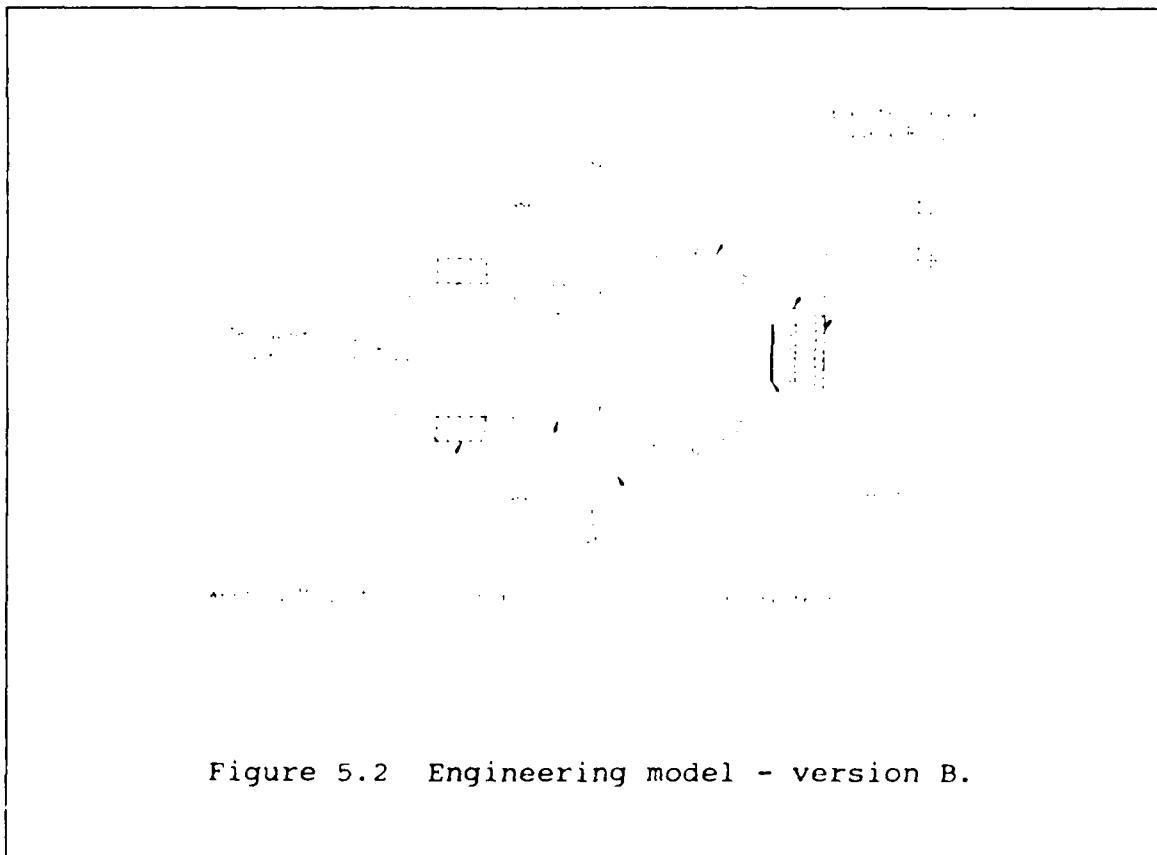


Figure 5.2 Engineering model - version B.

## 5.2 Performance Characteristics

The performance characteristics of the flight instrument can be estimated with the use of a simple model. In this model, three sources of experimental uncertainty are considered: the background counting rates of the SSD and the channeltron, and the true SSD-channeltron coincidences due to very low energy electrons, typically 1 to 10 eV, knocked out of the foil by the projectile. If  $R_p$  and  $R_H$  are the count rates in the SSD due to protons and hydrogen atoms incident on the entrance aperture of the instrument and  $RS_{BG}$  is the count rate due to all other causes, such as detector noise or high energy penetrating particles, then the total SSD count rate,  $R_{SSD}$ , is given by

$$R_{SSD} = R_p + R_H + RS_{BG} . \quad (5.1)$$

The total channeltron count rate,  $R_{CH}$ , is given by

$$R_{CH} = R_p Ne_p E + R_H Ne_H E + RC_{BG} + K \cdot (R_p + R_H) , \quad (5.2)$$

where  $Ne_p$  and  $Ne_H$  are the convoy electron yields per incident proton or hydrogen as given by eqs. (2.13) and (2.14),  $E$  is the instrumental efficiency of detecting a convoy electron,  $RC_{BG}$  is the channeltron background count rate and  $K$  is the probability of knockout from the foil and subsequent detection of a low energy electron. It is useful to define two parameters, the hydrogen-proton flux ratio,  $FR$ ,

$$R_H = FR \cdot R_p \quad (5.3)$$

and the proton-hydrogen convoy electron production ratio,  $CER$ ,

$$Ne_p = CER \cdot Ne_H . \quad (5.4)$$

For an actual flight instrument, taking data on orbit, both  $FR$  and  $CER$  are smaller than unity. Using eqs. (5.1) through (5.4) it is possible to write expressions for three quantities that describe the performance of the instrument: the true SSD-channeltron coincidence rate due to hydrogen atoms,  $C_{TH}$ ; the true coincidence

rate due to protons,  $C_{TP}$ ; and the accidental coincidence rate,  $C_A$ . These quantities are given by

$$C_{TH} = FR \cdot (R_p + R_H) \cdot (Ne_H \cdot E + K) / (1 + FR) \quad , \quad (5.5)$$

$$C_{TP} = (R_p + R_H) \cdot (CER \cdot Ne_H \cdot E + K) / (1 + FR) \quad (5.6)$$

and

$$C_A = [(1 + FR)R_p + RS_{BG}] \cdot [(FR + CER)R_p Ne_H E + RC_{BG} + (1 + FR)R_p K] \cdot \delta\tau \quad (5.7)$$

where  $\delta\tau$  is the coincidence resolving time.

The proposed flight instrument will be designed so that  $R_p$  will be of the order of  $10^3$  counts/sec,  $RS_{BG}$  will be negligible compared to  $R_p$  and the design goal for  $\delta\tau$  will be 100 nsec. The detection efficiency,  $E$ , is estimated to be 0.5. At a particle energy of 4 MeV and with a  $2 \mu\text{g}/\text{cm}^2$  carbon stripper foil, eqs. (2.13) and (2.14) give  $Ne_H = 0.267$  and  $CER = 1.3 \cdot 10^{-5}$ . Using these values in eqs. (5.5), (5.6) and (5.7) and neglecting, for the moment, the low energy electron contribution  $K$  yields:

$$C_{TH} = 150(FR + 1.3 \cdot 10^{-5}) \quad , \quad (5.8)$$

$$C_{TP} = 0.002 \quad , \quad (5.9)$$

and

$$C_A = (1 + FR)[0.013 \cdot (FR + CER) + 10^{-4} \cdot RC_{BG}] \quad (5.10)$$

If the minimum requirement is that the measured hydrogen coincidence rate is at least twice the random count rate then for a hydrogen to proton ratio,  $FR$ , of  $10^{-3}$  a channeltron noise count rate,  $RC_{BG}$ , as high as 750 Hz can be tolerated. It should be noted that while the channeltron noise,  $RC_{BG}$ , rate is roughly proportional to the area of the channeltron funnel, the electron collection efficiency,  $E$ , depends only on the electric field configuration in the instrument. Therefore, with a suitable choice of geometry and electrode voltages, it will be possible to maximize  $E$  even for a very small funnel, which will minimize the noise.



Low energy knockout electrons were a significant source of error for the electrostatic version of the instrument. Electron yields for the proton beams, listed in table 4.2, can be characterized by the following two observations: at any given energy the yield is independent of foil thickness and the yields, as a function of beam energy, are proportional to the energy loss of protons in carbon. These observations indicate that the charged beam electron yield is due to electrons knocked out of the foil in the last few atomic layers. These electrons have very low kinetic energies, of the order of a few eV, and, in principle, the grid located behind the carbon foil (Figure 3.3), held at -100 V with respect to the foil, should stop them from reaching the MCP. However, the grid was only a few millimeters from the foil and such a geometry leads to imperfect shielding. Some electric field lines that originate on the foil to bypass the grid and end on the MCP front plate. Low energy electrons are confined to motion along the field lines and, therefore, some low energy electrons will strike the MCP despite the grid shielding.

If the entire charged 4 MeV beam electron yield is due to these knockout electrons then the resulting value of  $K$  for the breadboard instrument is  $3.4 \cdot 10^{-3}$ . The geometry of the electric field lines between the foil and grid #1 in the engineering model (Figure 5.1) will be optimized to increase the shielding efficiency for low energy electrons. It should be possible to increase the efficiency by one to two orders of magnitude and, therefore, decrease the knockout electron detection probability,  $K$ , by a factor of 10 to 100.

Table 5.1 shows the effect of the projected improvement in knockout electron rejection on the instrument's sensitivity in distinguishing neutral particles from charged ones. The table is a list, for several values of  $K$ , of the minimum number of incident particles,  $N$ , required to detect a statistically significant signal for given value of the proton-hydrogen flux ratio,  $FR$ . The signal,  $D$ , is defined as the difference between the measured number of SSD-channeltron coincidences and the expected number of coincidences if there were no incident neutral particles. Statistical significance of the signal requires that  $D > \delta D$  where  $\delta D$  is the one standard deviation error in  $D$ .  $D$  is given by

$$D = C_{TH} + C_{TP} - C_{TP}^* \quad (5.11)$$

where  $C_{TH}$  and  $C_{TP}$  are the given by eqs. 5.5 and 5.6 respectively, with  $R_p + R_H = N$ , and  $C_{TP}^*$  is given by eq. 5.6, with  $R_p = N$ ,  $R_H = 0$ , and  $FR = 0$ . Since the  $C$  terms in eq. 5.11 are simply count rates, the error term,  $\delta D$ , is given by

$$\delta D = [C_{TH} + C_{TP} + C_{TP}^*]^{1/2} \quad (5.12)$$

Examination of values listed in Table 5.1 shows that, if good knockout electron rejection is obtained, values of the proton-hydrogen flux ratio as low as  $10^{-3}$  can be reliably measured with about  $10^4$  counts.

---

Table 5.1

Minimum number of incident particle counts required to determine a given neutral-charged particle flux ratio.

FR	N for		
	$K = 3.4 \cdot 10^{-3}$	$K = 3.4 \cdot 10^{-4}$	$K = 3.4 \cdot 10^{-5}$
$10^{-4}$	$3.8 \cdot 10^7$	$3.9 \cdot 10^6$	$4.8 \cdot 10^5$
$10^{-3}$	$3.9 \cdot 10^5$	$4.6 \cdot 10^4$	$1.1 \cdot 10^4$
$10^{-2}$	$4.6 \cdot 10^3$	$1.1 \cdot 10^3$	$8.0 \cdot 10^2$
$10^{-1}$	$1.3 \cdot 10^2$	$8.7 \cdot 10^1$	$8.2 \cdot 10^1$

---

## 6. CONCLUSIONS

An instrument designed to detect convoy electrons produced by particles with energies of the order of several MeV has been fabricated and successfully tested with neutral and charged beams of energies 1.5 to 4.0 MeV. Results of tests have shown that the instrument can distinguish between the two kinds of beams and this ability improves with increasing beam energy. Based on the experimental work described above, two preliminary designs for the engineering model of the neutral particle detector have been described. Evaluation of the designs indicates that neutral hydrogen to proton ratios, in the incident flux, as small as  $10^{-3}$  can be reliably measured. Detailed engineering model designs and a test program designed to evaluate the designs and finalize the flight model design will be submitted in a separate follow on proposal from Panametrics to the Geophysics Laboratory.

## REFERENCES

- 2.1) W. Brandt and R. Sizman, in Atomic Collisions in Solids, (Plenum, New York, 1975), Vol 1, p. 305.
- 2.2) C. K. Cline, T. E. Pierce, K. H. Purser and M. Blann, "Small Angle Scattering of  $^{32}\text{S}$  and  $^{16}\text{O}$  Beams in Thin Foils," Phys. Rev. **180**, 450 (1969).
- 2.3) M. J. Gaillard, J. C. Poizat, A. Ratkowski, J. Remillieux and M. Auzas, "Nonequilibrium Effects in the Proton Neutral Fraction Emerging from Solids Bombarded with MeV  $\text{H}^0$ ,  $\text{H}^+$ ,  $\text{H}_2^+$ , and  $\text{H}_3^+$  Beams," Phys. Rev. **A16**, 2323 (1977).
- 2.4) C. J. Powell, "Attenuation Lengths of Low-Energy Electrons in Solids," Surface Science **44**, 29 (1974).
- 2.5) R. Latz, J. Schader, H. J. Frischkorn, P. Koschar and K. O. Groeneveld, "Total Yield and Escape Depth of Electrons from Heavy Ion Solid Interactions," IEEE Trans. Nucl. Sci., **NS-30**, 913 (1983).